Structural Basis for Transfer RNA Aminoacylation by *Escherichia coli* Glutaminyl-tRNA Synthetase†

John J. Perona,‡ Mark A. Rould,§ and Thomas A. Steitz*

Department of Molecular Biophysics and Biochemistry and Howard Hughes Medical Institute, Yale University, New Haven, Connecticut 06511

Received February 1, 1993; Revised Manuscript Received June 1, 1993

ABSTRACT: The structure of *Escherichia coli* glutaminyl-tRNA synthetase complexed with $tRNA_2^{Gln}$ and ATP refined at 2.5-Å resolution reveals structural details of the catalytic center and allows description of the specific roles of individual amino acid residues in substrate binding and catalysis. The reactive moieties of the ATP and tRNA substrates are positioned within hydrogen-bonding distance of each other. Model-building has been used to position the glutamine substrate in an adjacent cavity with its reactive carboxylate adjacent to the α-phosphate of ATP; the interactions of the carboxyamide side chain suggest a structural rationale for the way in which the enzyme discriminates against glutamate. The binding site for a manganese ion has also been identified bridging the β- and γ-phosphates of the ATP. The well-known HIGH and KMSKS sequence motifs interact directly with each other as well as with the ATP, providing a structural rationale for their simultaneous conservation in all class I synthetases. The KMSKS loop adopts a well-ordered and catalytically productive conformation as a consequence of interactions made with the proximal β-barrel domain. While there are no protein side chains near the reaction site that might function in acid–base catalysis, the side chains of two residues, His43 and Lys270, are positioned to assist in stabilizing the expected pentacovalent intermediate at the α-phosphate. Transfer of glutamine to the 3′-terminal tRNA ribose may well proceed by intramolecular catalysis involving proton abstraction by a phosphate oxygen atom of glutaminyl adenylate. Catalytic competence of the crystalline enzyme is directly shown by its ability to hydrolyze ATP and release pyrophosphate when crystals of the ternary complex are soaked in mother liquor containing glutamine.

Crystallographic investigations are beginning to reveal in some detail the structural basis for catalytic function and tRNA discrimination by the aminoacyl-tRNA synthetases. This class of enzymes carries out the first step in protein synthesis by specifically coupling amino acids to their cognate tRNA acceptors [for a review, see Schimmel (1987)]. The crystal structures of *Escherichia coli* glutaminyl-tRNA synthetase (GlnRS; Rould et al., 1989), a tryptic fragment of *E. coli* methionyl-tRNA synthetase (MetRS; Brunie et al., 1990), and *Bacillus stearothermophilus* tyrosyl-tRNA synthetase (TyrRS; Brick et al., 1989) show that each possesses a canonical Rossmann fold domain containing the active site. Two conserved primary sequence motifs, designated by their single amino acid codes as HIGH and KMSKS, are located adjacent to the ATP binding site in each of these synthetases. The enzymes specific for glutamate (Breton et al., 1986), tryptophan (Hall et al., 1982), valine (Haertlein et al., 1987), isoleucine (Webster et al., 1984), leucine (Haertlein et al., 1987), arginine (Eriani et al., 1989), and cysteine (Eriani et al., 1991) also possess both of these sequence motifs. By contrast, the crystal structures of *E. coli* seryl-tRNA synthetase (SerRS; Cusack et al., 1990) and of *Saccharomyces cerevisiae* aspartyl-tRNA synthetase (AspRS; Ruff et al., 1991) show that the active site domains of these enzymes are structurally similar and consist of a seven-stranded antiparallel β-sheet flanked by α-helices. Several sequence motifs located adjacent to the catalytic sites are also found among eight other synthetases; together these 10 enzymes form a second subclass (class II; Eriani et al., 1990). Thus, separate and mutually exclusive sequence motifs divide the aminoacyl-tRNA synthetases into two classes, each of which possesses a unique structural fold in the catalytic domain.

The reaction catalyzed by aminoacyl-tRNA synthetases consists of a two-step process in which amino acids are first converted to aminoacyl adenylates in an activation step involving the cleavage of Mg^{2+}–ATP and subsequently transferred to tRNA (Schimmel, 1987). The use of phosphorothioate ATP analogs has shown that in solution the magnesium forms a bidentate complex with the β- and γ-phosphates of the ATP (Connolly et al., 1980; Smith & Cohn, 1982; Piel et al., 1983); Garcia et al., 1990). The *E. coli* GlnRS is one of only three synthetases that cannot carry out the activation of the amino acid in the absence of tRNA, suggesting that the active sites of these enzymes are not fully formed when tRNA is not present. Fersht and colleagues have utilized site-directed mutagenesis and linear free energy relationships to probe the energetics and mechanism of the TyrRS enzyme (Leatherbarrow & Fersht, 1986; Fersht, 1987). Many specific alterations were introduced into the enzyme on the basis of the crystal structure determined by Blow and co-workers (Brick et al. 1989), and analysis of the variants has allowed the conclusion that the activation of tyrosine by this enzyme results solely from the use of binding energy, without the direct involvement of covalent or acid–base catalysis due to enzyme functional groups. The functional consequences of mutation of basic residues present on two exposed loops near the active center were explained by the proposal that these loops undergo a conformational change to envelop the transition state of the reaction (Fersht et al.,

† This research was supported by the NIH.

* Author to whom correspondence should be addressed.

‡ Present address: Department of Pharmaceutical Chemistry, 926 Medical Sciences Building, University of California, San Francisco, CA 94143-0446.

§ Present address: Department of Biology, Massachusetts Institute of Technology, Cambridge, MA 02139.

0006-2960/93/0432-8758$04.00/0

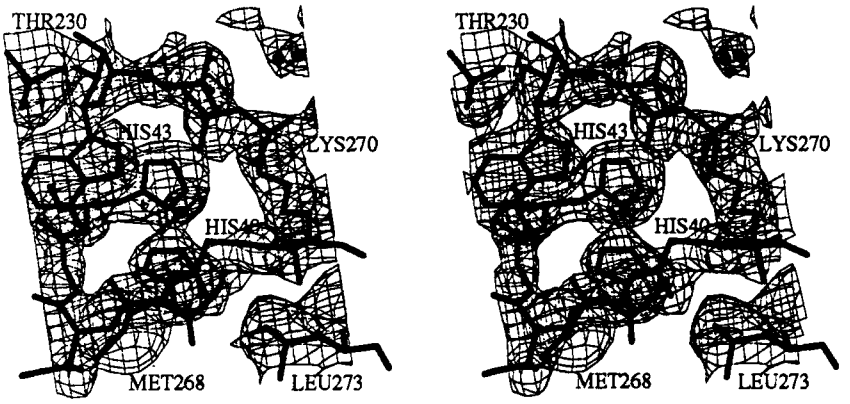

FIGURE 1: Divergent stereo view of an electron density map ($2F_o - F_c$) in the region of the active site. The map is contoured at 1.0σ; all residues containing at least one atom within 5 Å of any ATP atom were deleted from the model prior to refinement and map computation. This map includes structure factor amplitudes between 2.5- and 6.0-Å resolution and is calculated from native data collected at −20 °C in the presence of 20% glycerol. Note that under these conditions electron density is present for the side-chain nitrogen of Lys270. However, a similar omit map calculated at 2.8-Å resolution using the data collected at 8 °C indicates that this charged group is disordered (data not shown). While the lower temperature and/or presence of glycerol may contribute to the stabilization of this group, we expect that the improved refinement, including significantly more measured amplitudes, has allowed correct interpretation of its interactions with substrate and other enzyme groups. The refined coordinates of the GlnRS-tRNA^{Gln}–ATP ternary complex, determined from the low-temperature data, are otherwise very similar to those determined from data collected to 2.8-Å resolution at 8 °C (Rould et al., 1989). During the change in solution environment, a concerted motion of the entire structure by 0.4 Å occurs along the real-space *b*-direction, reflecting a small rearrangement of crystal packing contacts along this lattice axis. There is little perturbation of bound solvent structure as a consequence of the differing temperature/solution conditions used in the two crystal structures. Small differences in the conformation of the triphosphate moiety of ATP are observed between the two structural models, which results in slightly different interpretation of several enzyme–substrate contacts. The description in the text pertains to the 2.5-Å-resolution model throughout.

1988). The conserved KMSKS sequence motif is located on one of these loops; the lysine residues were proposed to interact directly with the transition state. Similar studies have implicated the second of these conserved lysine residues as critical to efficient catalysis by MetRS as well (Mechulam et al., 1991).

We have recently reported the structure of the *E. coli* GlnRS, a monomeric enzyme of 553 amino acids, complexed with tRNA^{Gln} and ATP (Rould et al., 1989, 1991). Here we describe the catalytic center of GlnRS in detail and compare its structure to that of TyrRS and MetRS. Direct interactions with polypeptide backbone groups account for the specificity of the enzyme for ATP. The 2′-OH of the terminal ribose group of the tRNA is positioned to facilitate attack on the α-phosphorus of the glutaminyl adenylate reaction intermediate, and a complementary binding pocket for the glutamine substrate exists in a position analogous to that of tyrosine in the homologous TyrRS. Interaction of the conserved HIGH and KMSKS motifs with each other as well as with the phosphates of ATP provides a structural rationale for their simultaneous conservation in all class I aminoacyl-tRNA synthetases. The detailed locations of His43 and Lys270 within these motifs suggest that each of these amino acids stabilizes the pentacovalent transition state at the α-phosphate during the formation of the glutaminyl adenylate intermediate.

MATERIALS AND METHODS

Refinement of the Ternary Complex to 2.8-Å Resolution. We have previously reported a preliminary refinement of the GlnRS-tRNA^{Gln}–ATP complex utilizing the program XPLOR, including two rounds of molecular dynamics-simulated annealing, which yielded a crystallographic *R*-factor of 27.9% for all data between 2.8- and 6.0-Å resolution (Rould et al. 1989). The two carboxyl-terminal β-barrel domains of the enzyme were partially disordered in this structure, and the interactions made by these domains with the anticodon nucleotides were not discernible. The data used in the structure determination were collected at a temperature of 8 °C in a stabilizing solution containing 56% ammonium sulfate, 80 mM PIPES buffer (pH 7.0), 30 mM $MgSO_4$, and 4 mM ATP. More recently, data collection carried out at −20 °C in a stabilizing solution containing 20% glycerol has allowed the measurement of diffraction applitudes to a resolution of 2.5 Å and has resulted in a clarification of the interactions made between the protein and anticodon loop of the tRNA (Rould et al., 1991). Refinement of the structure to 2.5-Å resolution has resulted in an *R*-factor of 21.0%, including 227 water molecules. This structure, with the omission of solvent, was used as a starting model for completion of refinement of the higher-temperature crystal structure to 2.8-Å resolution. The initial *R*-factor for the high-temperature data to 2.8-Å against the refined 2.5-Å resolution model was 31.2%, reflecting an approximately 1% change in cell dimension along the b^* reciprocal-space axis as a result of the differing solution/temperature conditions used in the two native crystals. All refinement was carried out with the program XPLOR (Brunger, 1988). Rigid body refinement of the entire complex as a single group, followed by positional refinement and refinement of tightly restrained individual *B*-factors, reduced the *R*-factor to 21.3%, with good stereochemistry. A total of 125 water molecules were then added by analysis of $(F_o - F_c)\varnothing_c$ maps and refined via positional refinement and refinement of tightly restrained individual *B*-factors. The final *R*-factor for the lower resolution model is 19.6% for all data in the resolution range 2.8–6.0 Å, with an rms deviation in bond lengths of 0.012 Å for both the protein and the tRNA and rms deviations in bond angles of 2.64° for the protein and 3.37° for the tRNA. Representative electron density for the higher resolution structure, upon which most interpretation is based, is shown in Figure 1.

Glutamine Binding Studies. Several approaches to preparing a crystalline complex of the enzyme that included glutamine were attempted in an effort to directly visualize the binding of this substrate (Table I). For each experiment, data were collected to the indicated resolution limit on the Xuong–Hamlin area detector system and reduced using the

Table I: Experimental Approaches for Characterization of Glutamine Binding

protocol	resolution (Å)	% complete	R_{merge} (%)[a]	R_{cross} (%)[b]	R_{cryst} (%)[c]
crystals soaked in solutions containing 20 mM glutamine	3.5–18	87	6.5	14.1	---
crystals grown in the presence of 4 mM ATP and 20 mM glutamine	3.5–18	96	10.1	10.8	---
crystals grown in the presence of 4 mM AMP and 20 mM glutamine	2.8–18	95	8.1	10.5	19.9

[a] $R_{merge} = (\sum|I_{i,n} - \langle I_n\rangle|)/\sum\langle I_n\rangle$, where $I_{i,n}$ is the ith observation of reflection n. [b] $R_{cross} = (\sum||I_n^{hkl}| - |I_d^{hkl}||)/\sum|I_n^{hkl}|$, where I_n^{hkl} is the native intensity, and I_d^{hkl} is the derivative intensity. [c] $R_{cryst} = (\sum_{hkl}||F_o^{hkl}| - |F_c^{hkl}||)/\sum_{hkl}|F_o^{hkl}|$, where F_o is the observed structure factor, and F_c is the calculated structure factor.

associated software developed by C. Nielsen. Data from crystals prepared from or soaked in solutions containing glutamine were local-scaled to native data to reduce any remaining systematic error due to absorption or crystal decay, and experimental difference maps using amplitudes ($2F_{Gln} - F_{Nati}$) and ($F_{Gln} - F_{Nati}$) were computed [F_{Nati} = native crystals composed of the ternary complex GlnRS-tRNA^{Gln}–ATP; F_{Gln} = native crystals modified (Table I) by solutions including the glutamine ligand]. Difference electron density maps computed with data collected from native crystals soaked in solutions containing glutamine, as well as from crystals grown in the presence of glutamine and ATP, used experimental MIR phases determined with the inclusion of constraints derived from solvent flattening (Rould et al., 1989). Difference electron density maps calculated with data collected from crystals grown in the presence of glutamine and AMP used calculated phases in the resolution range 2.8–6.0 Å and MIR phases for the lower resolution terms. Native crystals were grown as described (Rould et al., 1989) from solutions containing 48% ammonium sulfate as precipitating agent and were stabilized prior to soaking experiments in a solution containing 56% ammonium sulfate, 80 mM PIPES buffer (pH 7.0), 30 mM $MgSO_4$, and 4 mM ATP. Crystal growth in the presence of glutamine was carried out via hanging-drop vapor diffusion utilizing the same conditions as native (Table I).

Determination of the Structure of the GlnRS-tRNA^{Gln}–AMP Complex. Crystals grown in the presence of 4 mM AMP and 20 mM glutamine (Table I) were suitable for determination of the structure of the active site in the presence of the AMP product. The refined model of the ternary complex, as determined from the 2.8-Å native data, was used as a starting model for refinement. The β- and γ-phosphates of the ATP, as well as solvent molecules in the active site, were omitted from the model. The initial crystallographic R-factor was 25.4% for data in the resolution range 2.8–6.0 Å. The R-factor for these data was then reduced to 21.5%, with good stereochemistry, by positional refinement and refinement of tightly restrained individual B-factors. Repositioning of side chains and solvent molecules in the active site, followed by subsequent positional refinement and refinement of individual, tightly restrained B-factors, reduced the final R-factor to 19.9% for all data between 2.8- and 6.0-Å resolution. Deviations from ideal geometry were as follows: rms deviation on bond lengths = 0.012 for both the protein and the tRNA; rms deviation on angles = 2.68° for the protein and 3.38° for the tRNA.

Location of the Active Site Magnesium Ion. To allow interpretation of the positions of magnesium ions directly from difference electron density maps, data were collected to 3.5-Å resolution on crystals which were transferred through four changes of a solution containg 30 mM $MnSO_4$ and lacking added magnesium ions. Data were used to a resolution of 4.0 Å only, due to an increased sensitivity to radiation decay of the crystals (average decay in intensities was 30% in the resolution range from 4.0 to 18.0 Å). A merging R-factor

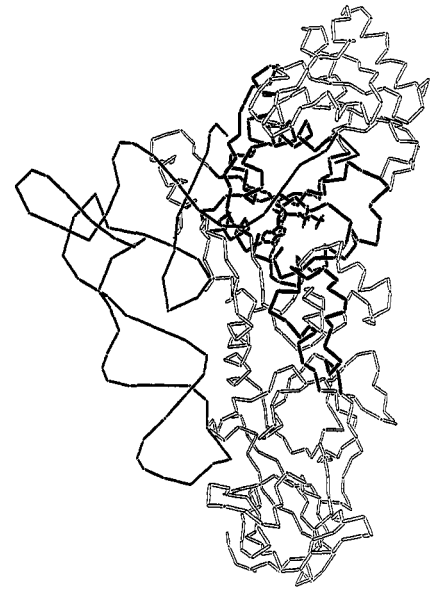

FIGURE 2: View of an α-carbon trace of glutaminyl-tRNA synthetase. The phosphate backbone of tRNA^{Gln} is shown in black; ATP is shown in the active site cleft. The canonical dinucleotide fold domain near the N-terminus is shaded. Two structural motifs (black), proposed to link the active site with regions of the protein-RNA interface involved in tRNA discrimination, are indicated. The α-helix (top) connects tRNA recognition in the minor groove of the acceptor stem with binding of the ribose group of ATP. The large loop (center) connects anticodon recognition by the two β-barrel domains (bottom) with sequences flanking the MSK sequence motif (see text), which interacts with the phosphates of ATP.

(Table I) of 6.7% for all data in this resolution range was calculated after data collection and reduction on the Xuong–Hamlin area detector. The data were local-scaled to native, and a cross R-factor (Table I) of 10.6% in this resolution range was calculated. Difference electron density maps were computed using coefficients $F_{Mn} - F_{Nati}$ as well as coefficients $F_{Mn(+)} - F_{Mn(-)}$ (where $F_{Mn(+)}$ and $F_{Mn(-)}$ are Friedel-related amplitudes) in order to exploit the anomalous scattering signal of the manganese ion. Experimentally determined MIR phases were used in computation of the maps; 90° was subtracted from all phases in the calculation of the anomalous difference Fourier map.

RESULTS

The structure of the ternary complex of GlnRS-tRNA^{Gln}–ATP at 2.5-Å resolution reveals that the α-phosphate of the ATP lies within hydrogen-bonding distance of the 2′-OH of nucleotide A_{76} of the tRNA; these two moieties are thus in proximity as required for their participation in the glutaminylation of the tRNA. Further, model-building suggests an orientation for the glutamine within a complementary enzyme cavity, such that the α-carboxylate lies adjacent to the α-phosphate of the ATP and the side chain makes specific interactions that may account for the enzymes' ability to discriminate between glutamine and glutamate. The positions

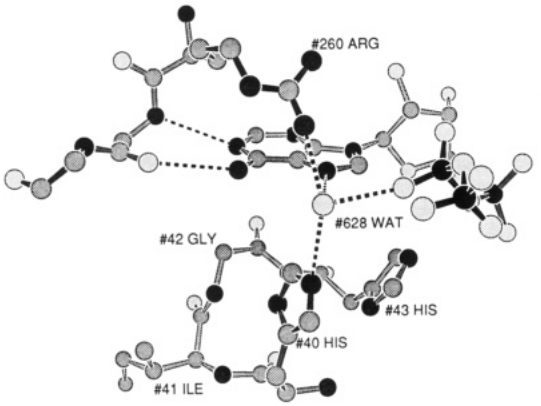

FIGURE 3: Polar and van der Waals interactions made by the adenine ring of the ATP. Hydrogen bonds are indicated by dashed lines. The centrally located water molecule (#628 WAT) accepts hydrogen bonds from Arg260 and His40 and is a hydrogen-bond donor to the N7 ring nitrogen and β-phosphate of the ATP. Viewed from this orientation, the α-phosphate is farthest to the right of the drawing.

of His43 and Lys270 relative to the α-phosphate of ATP suggest that these residues may directly stabilize the formation of the expected pentacovalent transition state. The active site is located at the C-terminal edge of a canonical 5-stranded parallel β-sheet structure (Rossmann fold, Figure 2), similar to its location in the structurally homologous TyrRS and MetRS enzymes. Two conserved sequence motifs are located in the active site in a similar though not identical way in these three crystal structures; in GlnRS they are observed to interact both with each other and with the ATP substrate, explaining their simultaneous conservation among all class I synthetases.

ATP Binding Site. Many of the interactions made by ATP occur with a β-strand–turn–α-helix motif located at the amino terminus of the dinucleotide fold (Figures 2–4). This motif forms part of a deep cleft in the enzyme that also provides the binding site for the ribose moiety of nucleotide A_{76} of the tRNA. However, a number of interactions made with the adenine ring and ribose of the ATP also occur with residues within the second half of the fold. Significant interactions are made as well with an enzyme loop (residues 260–270) which follows in sequence the last β-strand of the dinucleotide fold and which folds over the front of the binding site. In the presence of ATP, the active site cleft is also seen to provide binding sites for a number of well-ordered solvent molecules.

The specificity of the enzyme for ATP is a consequence of hydrogen-bonding interactions observed between the N1 and N6 of ATP and the peptide backbone amide NH and carbonyl oxygen of residue Leu261 (Figure 3). These interactions effectively discriminate against the binding of GTP and provide a structural basis for the observation (Schimmel & Söll, 1979) that synthetases have a specific requirement for ATP in the activation of the amino acid. The adenine ring is sandwiched between two moieties. It rests on the polypeptide backbone of the conserved Gly42 residue; any larger side chain at this position would cause steric interference with the ring (Figure 4). The aliphatic portion of the adjacent Arg260 residue in turn stacks on top of the adenine base, and a centrally located water molecule further bridges this guanidinium group to the β-phosphate of the ATP (Figure 3). Arg260 also adopts an alternative conformation at roughly 50% occupancy, in which it is oriented outside of the active site to interact with a bound sulfate anion located in a shallow depression on the enzyme surface. (The side chain of Lys272 also contacts this bound anion.) Interestingly, all three anticodon nucleotides are also recognized by extended polypeptide segments, in which the Watson–Crick moieties of each base are recognized by backbone atoms and an adjacent positively-charged residue interacts with the phosphate group of the RNA (Rould et al., 1991).

Both the His-Ile-Gly-His (residues 40–43) and Met-Ser-Lys (residues 268–270) motifs are located in the catalytic cleft of the enzyme. The imidazole rings of His40 and His43 are each oriented by means of hydrogen bonding to backbone amide groups along this portion of the sequence (Figure 4). Thus, the protonated nitrogen atom of each His is directed toward the negatively-charged ATP phosphates and acts as an obligate hydrogen-bond donor group. A bifurcated hydrogen-bonding interaction is made by His40 with the carbonyl group of Met268 and with the above-mentioned centrally located water (Figures 3 and 4), through which it bridges to the β-phosphate. The protonated nitrogen of His43 lies approximately 3.5 Å distant from a nonesterified oxygen atom of the α-phosphate, as well as from each of the oxygens linking to the ribose and β-phosphate moieties. The histidine rings are oriented roughly parallel relative to each other, and the side chain of Met268 packs underneath that of His40 (Figure 4). The interlocking HIGH and MSK structure motifs are further stabilized by two hydrogen bonds that link the main-chain carbonyl oxygen of His40 with the main-chain amide nitrogen atoms of His43 and Ala44, as well as a hydrogen bond between the main-chain amide nitrogen of Ile41 and the main-chain carbonyl oxygen of Pro291 within the helical subdomain. The side chain of Ile41 packs into the interior of the enzyme and provides a hydrophobic anchor for additional stabilization of the dual motif structure.

Lys270 within the MSK motif also interacts with the ATP phosphates (Figure 4). The positively-charged side-chain

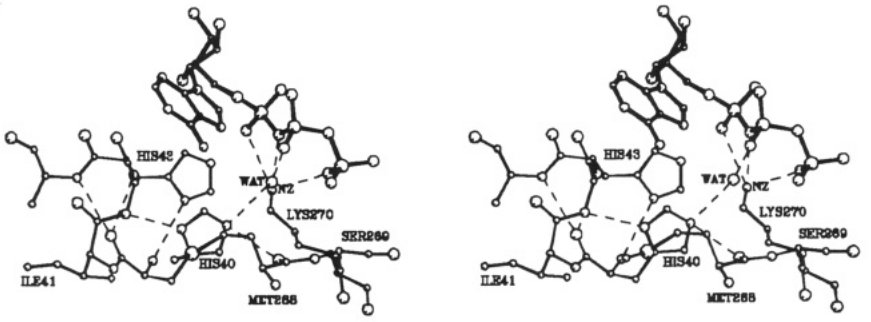

FIGURE 4: Divergent stereo view of the interactions made by the HIGH and KMSKS motifs with each other and with the ATP substrate. Distances measured between the protonated nitrogen atom of His43 and oxygens of the α-phosphate are too long to contribute significant binding energy (see text). The centrally located water molecule (WAT) is that also shown in Figure 3. The network of stabilizing hydrogen-bonding interactions is shown in dashed lines. Alternative sets of hydrogen bonds might also be made by the Nζ of Lys270, depending on the precise positioning of the protons as determined by rotation about the Cϵ–Nζ bond. Note that the interactions of Lys270 in this ternary ground-state complex differ from those proposed to obtain in the transition state (Figure 13a).

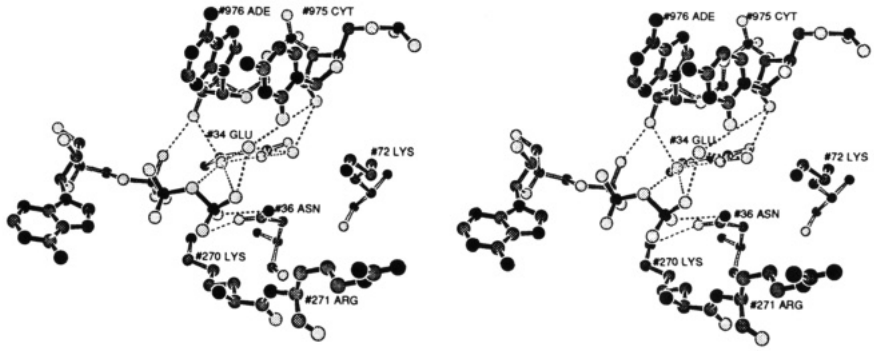

FIGURE 5: Divergent stereo view of further interactions in the active site. Ribose sugars of the 3′-terminal two nucleotides of $tRNA^{Gln}$ interact through water molecules (foreground) with protein residues as well as with the ATP. The side chain of Glu34 (background) plays a critical role in this complex hydrogen-bonding network by interacting with several waters, which in turn act as donors and/or acceptors to the ATP and tRNA. Dashed lines indicate hydrogen bonds. Several waters mentioned in the text are not shown for clarity.

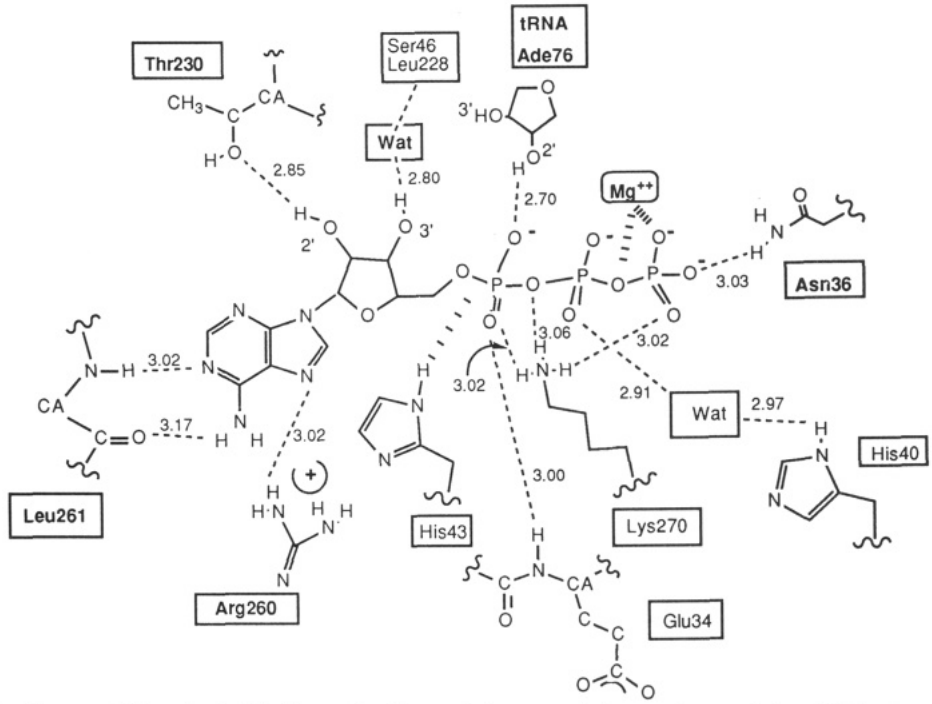

FIGURE 6: Schematic diagram of the principal hydrogen-bonding and electrostatic interactions made by ATP in the ternary complex with GlnRS and $tRNA^{Gln}$. Dotted lines indicate hydrogen-bonding or electrostatic interactions. Distances are indicated in angstrom units between the two electronegative atoms. The protonated nitrogen of His43 lies 3.4–3.5 Å from each of three oxygens bonded to the α-phosphorus atom. The proposed binding site for Mg^{2+} is also indicated.

amine group donates hydrogen bonds to a nonesterified oxygen of the α-phosphate and to the oxygen linking the α- and β-phosphates. The third hydrogen atom makes a bifurcated interaction with the γ-phosphate and the side-chain amide group of Asn36. Further stabilization of the ATP phosphates is provided by an additional hydrogen bond donated by the amide group of Asn36 to the γ-phosphate, as well as by several water-mediated hydrogen bonds involving Glu34 (Figure 5). Five water molecules also bind in this region of the active site, adjacent to the 3′-terminal adenosine of the tRNA. Two of these are located between the side chain of Glu34 and the base of nucleotide C_{75} of the tRNA. Another water molecule bridges the 3′- and 2′-OH groups of the ribose of nucleotide A_{76}; the latter of these ribose hydroxyls also makes hydrogen bonds with the α-phosphate of the ATP as well as with the two other water molecules (Figure 5).

The enzyme makes several polar intractions with the ribose ring of the ATP. Residue Thr230 emanating from the C-terminus of a β-strand within the second half of the fold interacts through its side-chain hydroxyl group with the 2′-OH of the ribose (Figure 6). A bound water molcule interacts with the 3′-OH of the ATP sugar and bridges this group to others on both sides of the fold. Thr230 is located on a short loop that bridges a β-strand and α-helix within the second half of the dinucleotide fold. This α-helix (α-helix H of the enzyme; Rould et al., 1989) lies in the minor groove of the tRNA acceptor stem. Residue Asp235 emanates from the helix to interact directly with the exocyclic N2 group of nucleotide G_3 of the tRNA in a sequence-specific manner (Perona et al., 1989). Thus, specific RNA discriminatory interactions are located on a polypeptide segment that is also directly involved in binding to the ATP substrate (Figure 2).

An additional structural feature of the active site also implies a linkage between tRNA selectivity and catalytic efficiency. Amino acids located immediately N- and C-terminal to the KMSKS motif make hydrophobic packing interactions with residues which form part of a large loop connecting two antiparallel β-strands of the proximal β-barrel domain of the enzyme (Rould et al., 1989). The tRNA anticodon binding site is located at the junction between the two C-terminal β-barrels. Specific recognition of the cognate anticodon might therefore trigger an allosteric response, resulting in recon-

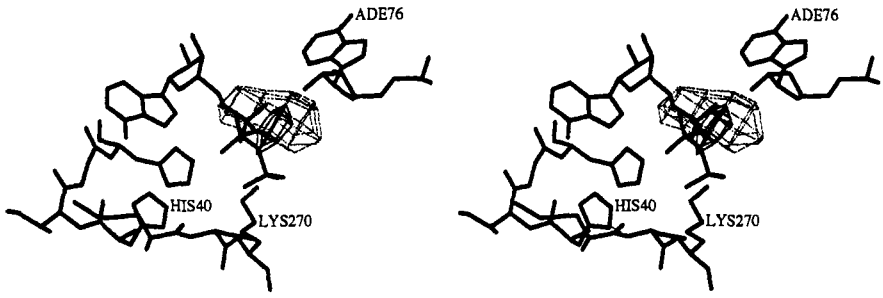

FIGURE 7: Difference maps calculated from native data and data collected from crystals soaked in solutions containing manganese ions. Difference electron density calculated with coefficients ($F_{Mn} - F_{nati}$) is shown in light lines; an anomalous difference electron density map calculated with coefficients ($F_{Mn(+)} - F_{Mn(-)}$) is shown in dark lines. Each map is countoured at 4σ and was calculated using structure factor amplitudes between 4.0- and 18-Å resolution. Experimentally determined MIR phases were used. The 3'-terminal A_{76} nucleotide of $tRNA^{Gln}$ is at the upper right.

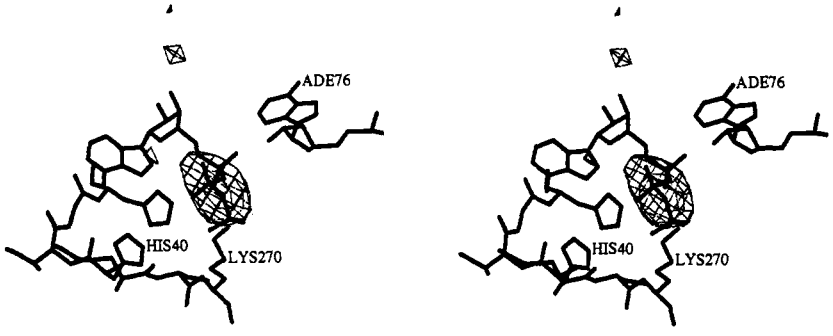

FIGURE 8: Difference electron density map calculated from coefficients ($F_{Gln} - F_{nati}$), where the F_{Gln} were measured from crystals of the ternary complex soaked in 20 mM glutamine. The map is contoured at -4σ and was calculated using structure factor amplitudes between 3.5- and 18-Å resolution. Experimentally determined MIR phases were used. The large hole at the position of the β- and γ-phosphates indicates that the crystalline enzyme is catalytically active.

figuration of the active site some 35 Å distant (Figure 2; Rould et al., 1991).

Magnesium Binding Site. The position of an exchangeable magnesium ion has been found by soaking native crystals in solutions containing ATP and 20 mM $MnSO_4$ and lacking added magnesium ions. The divalent manganese ion can readily substitute for magnesium, allowing the location of binding sites directly from difference electron density maps. The observation that these crystals are capable of catalyzing the activation of glutamine, with concomitant release of pyrophosphate (see below), supports the contention that magnesium must bind in the proximity of the ATP. Both isomorphous and anomalous difference electron density maps calculated at 4-Å resolution from data obtained under these conditions show a very large peak between the β- and γ-phosphates of the ATP on the side opposite nucleotide A_{76} of the tRNA (Figures 6 and 7). This peak represents the best candidate for the binding site of the catalytic magnesium ion. Although we do not observe an electron density peak at this position in the native maps, magnesium may bind less tightly to this site than does manganese under the high ammonium sulfate conditions which stabilize the crystals.

Glutamine Binding Site. Although we have no direct structural information on the location of the glutamine substrate in these cocrystals, data obtained from crystals in which all three of the substrates ATP, glutamine, and tRNA are present demonstrates that productive binding of glutamine does occur and that the enzyme is catalytically active in this crystal lattice environment. Difference electron density maps calculated from data obtained either from cocrystallization of glutamine and ATP with the enzyme–tRNA complex or from soaking of the GlnRS-tRNA–ATP crystals in solutions containing glutamine (Table I) show the presence of a large hole at the position of the β- and γ-phosphates of the ATP, indicating that these moieties are no longer present (Figure 8). Since an analogous feature suggesting spontaneous ATP hydrolysis has never been observed in native electron density maps, even when data were obtained from crystals up to 1 year old, we conclude that the enzyme in this lattice environment possesses catalytic activity. The observed hole is presumably a consequence of enzymatic formation of glutaminyl adenylate and pyrophosphate with the subsequent dissociation of the latter. We do not observe, however, any electron density corresponding to the presence of glutamine under either of these experimental conditions. It is possible that the unstable glutaminyl adenylate, once formed, is hydrolyzed to glutamine and AMP with consequent dissociation of the glutamine. Alternatively, the activated glutamine may be transferred to the 2'-OH group of the ribose of nucleotide A_{76} of the tRNA. Subsequent to this, the aminoacyl bond, which is known to be labile at neutral and basic pH, may be hydrolyzed.

Electron density maps of the ternary complex GlnRS-$tRNA^{Gln}$–AMP, calculated from data obtained from crystals which were grown in the presence of AMP and glutamine (Table I), also fail to reveal evidence for binding of glutamine in the active site cleft. Simultaneous binding of glutamine and AMP does not occur during the kinetic pathway of aminoacylation; unfavorable juxtaposition of the negatively-charged carboxylate and phosphate groups may prevent these two ligands from binding together. A number of additional soaking and cocrystallization experiments, some involving nonreactive analogs of ATP and glutamine, were also unsuccessful in delineating the glutamine binding site. In each experiment, either the glutamine concentration is significantly below its binding constant under the conditions used or it is bound but disordered within the binding pocket.

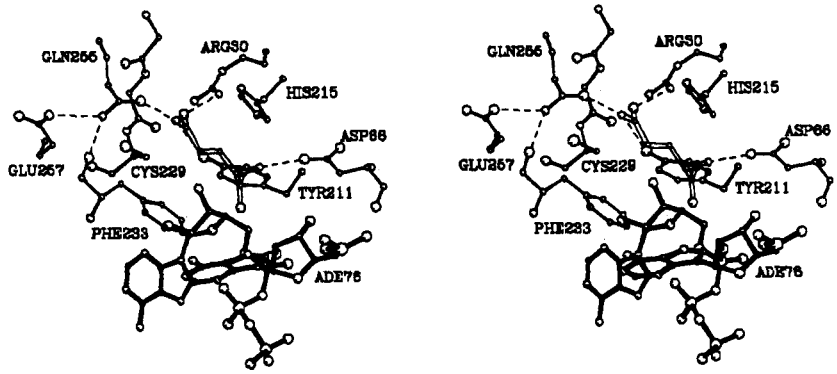

FIGURE 9: Divergent stereo view of the crystal structure of the active site region adjacent to the ATP binding site, showing a model-built glutamine substrate (open lines) making many interactions with various enzyme groups. ATP (bottom) and the terminal A_{76} nucleotide of the tRNA are shown in heavy lines. Dotted lines indicate proposed hydrogen-bonding interactions between the enzyme and glutamine substrate. The model of glutamine was constructed by interactively adjusting the position of the carboxyamide side-chain group to achieve hydrogen-bonding interactions with the side chains of Arg30, Gln255, and Tyr211. Subsequent to positioning the side-chain group, torsion angles of the aliphatic chain were systematically altered to achieve optimal interaction of the NH_3^+ group with the carboxylate of Asp66. The proposed hydrogen bond between substrate glutamine and Gln255 may be weak owing to an unfavorable geometry; however, it could be improved by small conformational adjustments in the Gln255 side chain as a response to glutamine binding. The guanidinium group of Arg64 (not shown for clarity) lies directly behind the His215 side chain at a distance of approximately 3.5 Å.

The structure of the active site cleft in the presence of ATP and the 3′-end of the transfer RNA reveals an additional unoccupied pocket adjacent to the α-phosphate of the ATP and the ribose of nucleotide A_{76} of the tRNA, which provides a likely binding site for the glutamine substrate (Figure 9). This cavity is formed from residues in both the first and second halves of the dinucleotide fold. Modeling the substrate glutamine into the pocket (Figure 9, legend) shows that the positively-charged α-NH_3^+ group is readily positioned to make a salt bridge to the side-chain carboxylate of Asp66. Significantly, this residue is conserved as either an Asp or Glu in all class I aminoacyl-tRNA synthetases, although its position in the sequence differs for TyrRS [see Discussion and Landes et al. (1993)]. Pro32 forms a platform upon which are stacked the α- and β-carbons of the glutamine. The remainder of the substrate is wedged between the side chains of Cys229 and His215 and makes hydrogen-bonding interactions with the side chains of Arg30, Gln255, and Tyr211 (Figure 9). Tyr211 and Phe233 form a hydrophobic "lid" to the binding site; these aromatic groups also provide stacking interactions with the adenine ring of the 3′-terminal A_{76} of the tRNA. Interactions of the NH_2 moiety of Gln255 with the carboxylate of Glu257 and the main-chain carbonyl group of Phe233 serve to orient the carboxylamide as a hydrogen-bond acceptor from the glutamine substrate.

Discrimination against productive binding and acylation of glutamate by GlnRS must rely on the differences between the uncharged carboxylamide glutamine side chain and the negatively-charged carboxylate of glutamate. Placement of a negatively-charged oxygen atom of glutamate adjacent to Tyr211 and Gln255 (Figure 9) would be less favorable than the NH_2 group of glutamine, owing to electrostatic repulsion from the oxygen of the Gln255 side chain. However, other more subtle mechanisms may also provide for discrimination. For example, binding of glutamate might propagate a conformational change in the enzyme, resulting in mispositioning of the reactive moieties of the substrates with respect to each other. One easily envisaged mechanism for this could be through elevation of the pK_a of His215, causing an unfavorable juxtaposition with the positively-charged Arg30 and Arg64 side chains (Figure 9, legend).

With the exception of the reactive carboxylate group, there are no unfavorable steric clashes between the modeled glutamine and groups on the enzyme. The carboxylate does make several short contacts with the ribose of ATP and the Pro32 ring (Figure 9). Further, the nucleophilic oxygen of this group is located 3.6 Å from the α-phosphorus atom of ATP and is displaced from a direct in-line position as required by the reaction stereochemistry. This suggests that some structural rearrangements must occur in the course of productive binding of both glutamine and ATP (see Discussion). The binding site for glutamine is located deep in the active site cleft beneath the ATP; this position suggests that glutamine is likely to bind prior to ATP in an ordered mechanism. If this is so, the hydrolysis of pyrophosphate upon soaking of the crystals in solutions containing glutamine can be explained by the fact that ATP is in equilibrium between bound and unbound states, thereby allowing entry of the glutamine.

Structure of the GlnRS-tRNA^{Gln}–AMP Ternary Complex. The structure of the active site of GlnRS in the presence of the product AMP, as determined from crystals grown in the presence of this product and glutamine, reveals that there is little structural perturbation which arises as a result of the absence of the β- and γ-phosphates. All of the interactions involving the adenine ring of the substrate are conserved. A small rotation of the α-phosphate relative to its position in the ATP occurs, which results as well in a small reorientation of the ribose ring. As a consequence of these structural changes, the 3′-OH of the ribose makes a new hydrogen-bonding interaction with the side-chain hydroxyl group of Ser46 (Figure 10). A significant rotation about the Cα–Cβ bond of the serine occurs to allow this interaction. The other interactions made by the 2′-OH and 3′-OH of the ATP are conserved, although some of the hydrogen-bonding distances are slightly altered.

A large solvent molecule, most likely a sulfate anion, binds in the approximate location of the γ-phosphate of the ATP. An additional water molecule is present at the site vacated by the β-phosphate of the ATP; it forms hydrogen bonds to the phosphate of AMP and to the centrally-located water which bridges to Arg260 and His40 (Figures 3,4). Several of the other water molecules which bind in the presence of ATP either are less well-defined and not unambiguously evident in the electron density maps or adopt alternative hydrogen-bond donor/acceptor interactions (Figure 10). The terminal NH_3^+ group of Lys270 is well-ordered and donates hydrogen bonds to the AMP phosphate group, the main-chain carbonyl group

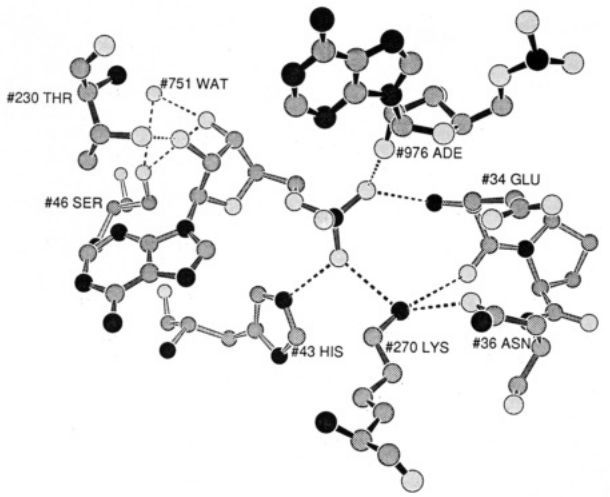

FIGURE 10: Interactions between AMP and the enzyme observed in the ternary complex GlnRS-tRNA^{Gln}–AMP. This structure was determined from data collected from crystals of the enzyme–tRNA complex cocrystallized in the presence of AMP and glutamine. Note the direct hydrogen bond made by Ser46 with the 3′-ribose group of the AMP and the good hydrogen bonds formed by the phosphate group with His43 and Lys270. His43 does not interact strongly with the α-phosphate of ATP in the ground-state complex.

of Glu34, and the side-chain amide oxygen of Asn36. Arg260 again adopts the same two conformations, with little preference observed for location of the side chain inside or outside the binding pocket.

DISCUSSION

Structural Comparisons among GlnRS, TyrRS, and MetRS. It is of interest to compare in detail the structures of the homologous active site regions of GlnRS, TyrRS, and MetRS. As members of the class I synthetase family, these three enzymes presumably arose from a common ancestor. They have retained many common features (for example, the use of Mg^{2+}–ATP as high-energy cofactor) but have also acquired impressive selectivities in their productive binding of specific amino acid and tRNA molecules. The homologous structures of the active site-containing Rossmann folds of the enzymes and the conservation of the HIGH and KMSKS motifs lead to the strong expectation that the ATP and amino acid substrates should bind similarly. It is notable that each of the crystal structures of the three enzymes represents a different step in the overall mechanism: GlnRS is cocrystallized with tRNA and ATP as well as tRNA and AMP (Rould et al., 1989); the TyrRS crystal structures have been solved in the presence of tyrosyl adenylate, tyrosinyl adenylate, and tyrosine (Brick et al., 1989; Brick & Blow, 1987); and the MetRS structure was determined from native crystals soaked in solutions containing ATP (Brunie et al., 1990). Interpretation of these differing ligand-binding states with a view toward conservation of the overall reaction provides increased insight into the structural and mechanistic basis of enzymatic function.

Overall Structure of the Dinucleotide Fold. The dinucleotide fold domains of GlnRS, MetRS, and TyrRS are structurally superimposable; each pairwise comparison of the three enzymes yields an rms deviation in position of equivalent α-carbon atoms of approximately 1.7 Å (Table II; Brunie et al., 1990; Perona, et al., 1991). Structural similarities among the three enzymes lie predominantly within the defined secondary structure elements of the fold, with variability in the sizes and conformations of the loops bridging these segments (Table II).

Table II: Superposition of α-Carbon Atoms within the Dinucleotide Fold Domains of TyrRS and GlnRS[a]

trial structure (TyrRS)		reference structure (GlnRS)			
residues	secondary structure	residues	secondary structure	no. of residues	rms D^b (Å)
30–34	β-B	26–30	β-1	5	1.65
36–40	β-B	32–36	β-1	5	1.49
43–55	loop,α-H3	38–50	loop,α-B	13	1.03
62–71	β-C	58–67	β-2	8	1.63
95–105	α-H5	75–85	α-C	11	1.83
121–126	β-D	97–102	β-3	6	1.58
170–173	α-H10	212–215	α-G	4	2.55
184–197	β-E	222–235	β-9	14	2.04
201–209	α-H11	239–247	α-H	9	2.00
216–222	β-F	254–260	β-10	7	1.21
overall equivalence:				84	1.73

[a] Structural superpositions were carried out by the program OVRLAP, which implements the algorithm of Rossmann and Argos (1976). An initial equivalence of six residues in the region of the HIGH motif was provided, and α-carbons 20–260 of GlnRS and 20–222 of TyrRS were included in the comparison. Secondary structure designations follow those of Rould et al. (1989) and Brick et al. (1989) [β: β-strand; α: α-helix]. [b] Root mean square deviation.

The dinucleotide fold of TyrRS possesses a sixth parallel β-strand formed from residues at the extreme amino terminus of the enzyme; this additional strand lies adjacent to strand β-F at the carboxyl end of the second half of the fold. Both GlnRS and MetRS also possess a sixth parallel β-strand at this position, but in these two enzymes it follows strand β-F in sequence and is linked to it via a left-handed connection. This disparity is of functional significance: the left-handed connective loop and sixth β-strand form part of an α-helix–turn–β-strand–α-helix motif which is conserved in structure between GlnRS and MetRS (Perona et al., 1991). In GlnRS this motif interacts with the inside corner of the "L" of the tRNA and serves to globally position this substrate on the surface of the enzyme. Accordingly, modeling has shown that MetRS and GlnRS may well bind their cognate tRNA substrates in very similar overall orientations (Perona et al., 1991). By contrast, elegant experiments have demonstrated that the TyrRS dimer binds a single tRNA molecule which spans the two subunits, giving rise to "half-of-the-sites" reactivity (Carter et al., 1986). This precludes binding of the tRNA in an orientation similar to that of GlnRS and therefore indicates a correlation between the connectivity of the sixth β-strand of the dinucleotide fold and the overall topology of tRNA binding.

The dinucleotide folds of each enzyme also possess an inserted domain, which in GlnRS binds a hairpinned conformation of the acceptor end of the tRNA (Rould et al., 1989). In TyrRS this insertion contains just 45 amino acids, less than half the number in GlnRS and MetRS. The TyrRS inserted domain also lacks a 24 amino acid section of structural similarity present in GlnRS and MetRS (Perona et al., 1991), which consists of an α-helix–turn–β-strand motif that wraps around the back side of the domain. This conserved motif may stabilize the overall domain structure for its function in binding the 3′-end of the tRNA. Despite the absence of structural similarity, the inserted domain of TyrRS nonetheless also plays a role in properly orienting the 3′-end of the tRNA substrate. Site-directed mutagenesis and molecular modeling have shown that basic residues within this domain interact with the phosphates of the acceptor strand. This information has been used to trace the path of the polynucleotide backbone across the enzyme surface (Bedouelle & Winter, 1986;

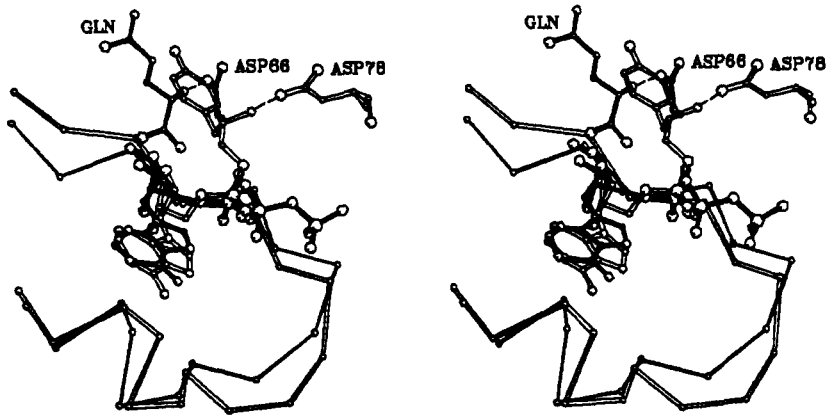

FIGURE 11: Superposition of ligands in the active site regions of GlnRS (dark lines) and TyrRS (open lines). The α-carbon traces correspond to β-strand 1 and α-helix B of GlnRS (Table II). Superposition of the tyrosyl adenylate was carried out by applying the coordinate transformation used to superimpose the entire nucleotide fold of TyrRS upon that of GlnRS. The relative positions of Asp66 of GlnRS and Asp78 of TyrRS (each interacting with the α-NH_3^+ group of the amino acid substrate) are shown together with the modeled position of the glutamine substrate (GLN) bound to GlnRS.

Labouze & Bedouelle, 1989). The acceptor stem of the tRNA approaches the active site from a quite different direction as compared to the binding of the 3′-end of $tRNA^{Gln}$ to GlnRS. The model is consistent with evidence that the TyrRS enzyme binds a single tRNA across a dimer interface formed by the inserted domain (Carter et al., 1986; Brick et al., 1989). The widely differing sizes and structures of the inserted domain between GlnRS/MetRS and TyrRS are thus likely to reflect in part the need to accommodate the large difference in the overall orientation of tRNA binding to these enzymes.

ATP and Amino Acid Binding Sites. Structural superposition of the Cα backbone atoms of the dinucleotide fold shows that the adenine ring, ribose, and α-phosphates of ATP and of tyrosyl adenylate bind in very similar orientations to GlnRS and TyrRS, respectively (Figure 11). Whereas the HIGH motif adopts a similar orientation in the two enzymes, the loop containing the MSK sequence (which follows the last β-strand of the fold and folds over the front of the binding cleft) differs markedly in conformation. However, kinetic data indicate that Lys230 and Lys233 of the KMSKS motif stabilize the transition state in TyrRS (Fersht et al., 1988). Therefore, this loop must alter its conformation upon binding ATP and during the course of tyrosyl adenylate formation, moving toward the active site so as to allow the lysine side chains to interact with the ATP phosphates. This suggests the possibility that when both ATP and tyrosine are bound, the KMSKS loop of TyrRS could adopt a structure similar to that seen in the GlnRS cocrystals. The catalytic conversion of ATP to AMP by crystalline GlnRS in the presence of glutamine supports the contention that the conformation of the KMSKS loop seen in the cocrystal structure with tRNA is identical or very similar to that which may be catalytically productive in both enzymes.

The most likely explanation for the adoption of a catalytically productive conformation of the KMSKS loop in GlnRS is the presence of tRNA in the crystals. Binding of the cognate tRNA anticodon loop to the C-terminal β-barrel domains of GlnRS has been hypothesized to transmit an allosteric signal by means of the large loop connecting two of the antiparallel β-strands of the proximal domain, which packs directly on residues flanking the KMSKS motif (Figure 2, Rould et al., 1991). In the absence of interactions with the tRNA anticodon, this large loop could well adopt a different conformation which fails to stabilize the productive conformation of the KMSKS motif. The observation that mutations in the anticodon loop of $tRNA^{Gln}$ cause very large decreases in the k_{cat} for aminoacylation is consistent with the hypothesis that there is an allosteric interaction between the anticodon binding site and the active site (Jahn et al., 1991). Further, the crystal structure of GlnRS cocrystallized with $tRNA^{Gln}$ and AMP shows that the productive conformation of the KMSKS loop is maintained in the absence of the β- and γ-phosphates of the ATP, suggesting that these moieties are not critical to adoption of the catalytically competent structure in GlnRS.

It is important to note also that GlnRS requires tRNA binding in order to synthesize glutaminyl adenylate, whereas the activation of tyrosine by TyrRS proceeds in the absence of $tRNA^{Tyr}$ (Schimmel & Söll, 1979). The factors that stabilize the productive conformation of the KMSKS loop are thus likely to be different in the two enzymes. Binding of ATP and/or tyrosine alone must be sufficient to cause the KMSKS loop of TyrRS to adopt the catalytically active conformation, which rearranges after formation of tyrosyl adenylate to the structure seen in the cocrystals with this intermediate. By contrast, the requirement for tRNA binding to GlnRS in order to allow enzymatic activation of glutamine may be related to a role in stabilizing the required conformation of the KMSKS loop.

A number of structurally equivalent residues in GlnRS and TyrRS (Table II) have the same function in ligand binding. In GlnRS, the main-chain amides of Glu34 and Thr230 donate hydrogen bonds to the α-phosphate and O2′-ribose of ATP, respectively (Figures 5 and 6); the equivalent Asp38 and Gly192 of TyrRS perform the same function (Brick et al., 1989). Similarly, in both enzymes the O3′-ribose hydroxyl bridges through a water molecule to residues on each half of the fold. However, a number of important differences are also seen. In the TyrRS cocrystal structure with tyrosyl adenylate, no polar interactions are made with the adenine ring, in contrast to the hydrogen bonds formed by Arg260 and the Leu261 main chain of GlnRS with the N7, N1, and N6 nitrogens. It is thus not clear how TyrRS discriminates against GTP binding, since there also appears to be no steric hindrance to the presence of an exocyclic nitrogen at the 2-position of the ring (Brick et al., 1989). ATP bound to TyrRS may make discriminatory interactions similar to those made with GlnRS, but after reaction with tyrosine the adenine ring of tyrosyl adenylate could be displaced from this initial position to accommodate interactions made by the tyrosine group. Consistent with this hypothesis are structural differences observed at residues 221–223 (equivalent to 259–261 of

FIGURE 12: Divergent stereo drawing of the superposition of α-carbon atoms of GlnRS (dark lines) and MetRS (open lines) in the region of the active site. The side chains of the conserved second lysine residue of the KMSKS sequence motif (Lys270 of GlnRS; Lys335 of MetRS) are seen to be adjacent to the phosphate groups of the respective ATP substrates. The β-strand–turn–α-helix motif shown represents a structurally homologous region found at the amino terminus of the first half of each dinucleotide fold (residues 27–57 of GlnRS and 7–38 of MetRS) and contains the conserved HIGH motif at the amino terminus of the α-helix. For each enzyme, the superimposed β-strand at left precedes directly in amino acid sequence the KMSKS motif and represents the last structural element of the second half of the fold (residues 254–261 of GlnRS and 319–326 of MetRS; Perona et al., 1991).

GlnRS) between the structures of TyrRS complexed with tyrosine and with tyrosyl adenylate. In the former structure the backbone bends inward, resulting in positioning of the discriminating carbonyl oxygen considerably closer to its position in GlnRS (Brick et al., 1989; Brick & Blow, 1987).

A second structural difference of importance involves stabilization of the ATP phosphates by ionic interactions with basic residues of the enzymes. In TyrRS both Lys230 and Lys233 of the KMSKS motif are proposed to interact with the transition state of the reaction. GlnRS lacks the first of these lysine residues; however, Arg260 may play an analogous role by interacting with the β-phosphate through a water molecule. Lys82 and Arg86 of TyrRS have been shown to provide further stabilization of the transition state for the activation of tyrosine (Fersht et al., 1988). These residues are located on a 23 amino acid flexible loop which follows strand β-C of the dinucleotide fold. Inspection of the GlnRS structure shows that Arg271 and Lys72 are solvent-accessible amino acid located adjacent to the ATP (Figure 5). While neither of these residues interacts with the ATP in this ground-state structure, modeling suggests that conformational changes of the side chains could allow them to interact directly with the transition state. Thus, the common need of the two enzymes to bind and orient the ATP phosphates is met by similar ionic interactions with basic residues, but the positions of these amino acids in the sequence are not strictly conserved.

A striking divergence in the binding of the amino acid substrate involves Asp78 of TyrRS, which is also located on the large flexible loop following strand β-C of the fold. This amino acid stabilizes tyrosine binding through formation of an ion pair with the α-NH_3^+ group of the substrate (Figure 11). The model of glutamine bound to GlnRS involves a similar ion pair interaction of the α-NH_3^+ group with Asp66, which is located at the C-terminus of strand β-2 of the dinucleotide fold (Figures 9 and 11). The proposed role of this amino acid in GlnRS is supported by its conservation as an acidic residue in the same sequence position in all but one of the other class I synthetases (Landes et al., 1993). TyrRS is the exception because Asp78 is not located in a structurally equivalent position—it is found on a connecting loop rather than a β-strand of the fold.

Superposition of GlnRS and TyrRS reveals that Asp78 of TyrRS occupies the same position as does nucleotide A_{76} of $tRNA^{Gln}$. The side chain of Asp78 extends toward the phosphate of tyrosyl adenylate and interacts with the α-NH_3^+ group of this reaction intermediate. The α-phosphate of ATP bound to GlnRS superimposes well with the phosphate of tyrosyl adenylate, and the carboxylate of Asp66 projects in that direction from the opposite side to form the ion pair with the α-NH_3^+ group of the modeled glutamine (Figure 11). Thus, the side chains of Asp66 of GlnRS and Asp78 of TyrRS may perform identical functional roles in stabilizing substrates that are bound in similar orientations, despite being located in different relative positions in the sequence. This is made possible by the differing modes of binding of the acceptor strand of the respective tRNAs, which allows Asp78 of TyrRS and nucleotide A_{76} of $tRNA^{Gln}$ to occupy the same position. It is worth noting that, with the possible exception of TrpRS, TyrRS is the only class I synthetase that binds tRNA across two subunits as well as the only one that diverges in the position of the conserved aspartate or glutamate.

The proposed glutamine binding site in GlnRS is adjacent to but does not superimpose directly with that of tyrosine in TyrRS (Figure 11). This is correlated with the fact that the relative positions of Asp66 of GlnRS and Asp78 of TyrRS differ despite a likely common role in binding the α-NH_3^+ group of the substrate in each case. The position of the modeled glutamine side chain is related to that of the tyrosine ring by rotation of about 100° around the bond joining the α-carbon and carboxylate carbon atoms. This difference arises as a

consequence of optimizing the interaction of the α-NH_3^+ group with Asp66. The binding pocket for tyrosine in TyrRS is in fact quite broad and binds several water molecules in the presence of the substrate; the modeled glutamine occupies a position more closely analogous to these waters.

Comparison of the active site structures of MetRS and GlnRS reveals that ATP diffused into MetRS crystals binds to this enzyme quite differently than to GlnRS (Figure 12; Brunie et al., 1990). Only the relative positioning of the ATP phosphates and the second lysine residue of the KMSKS motif is loosely related. This alternative orientation has been interpreted to mean that MetRS binds both ATP and (necessarily) methionine in a structurally different manner despite the structural and sequence homology of the dinucleotide fold domains of the group I synthetases (Brunie et al., 1990). Some divergence in the modes of substrate binding has clearly occurred in this class of enzymes, as evidenced by the expected differing orientation of the acceptor strand of $tRNA^{Tyr}$ bound to TyrRS. However, a discriminatory binding pocket for the methionine substrate, which would also permit juxtaposition of its carboxylate group with the α-phosphate of ATP, is not evident in the structure.

It is our strong expectation that the residues of the HIGH and KMSKS motifs that are conserved in the 10 class I synthetases will have identical interactions and functions in binding the phosphates of ATP. Therefore, the exact way in which the second (strictly conserved) lysine of the KMSKS motif stabilizes the pentacovalent transition state (see below) is predicted to be identical in each enzyme. ATP was bound to MetRS crystals by soaking it into the preexisting crystal lattice rather than by cocrystallization as was the case for GlnRS. Thus, it is possible that the crystal lattice precludes the adoption of the catalytically active complex of ATP bound to the enzyme; therefore, the observed mode of binding may, in fact, represent a nonproductive complex in this experimental system. Additional crystallographic studies on the interaction of MetRS cocrystallized with its substrates will be necessary to resolve this issue.

Catalytic Mechanism of Glutaminyl-tRNA Synthetase. Aminoacyl-tRNA synthetases catalyze formation of the aminoacyl ester bond linking the amino acid and tRNA substrates by a two-step mechanism: activation of the amino acid as aminoacyl–AMP followed by subsequent transfer of the aminoacyl group to one of the ribose hydroxyls of nucleotide A76 of the tRNA (Schimmel & Söll, 1979; Figure 13). Although the mechanistic details of the reaction catalyzed by GlnRS have not not been investigated, studies on a number of other synthetases have shown that activation of the amino acid proceeds by an in-line displacement reaction, resulting in inversion of stereochemical configuration at the α-phosphorous (Lowe & Tansley, 1984; reviewed in Cullis, 1987). In this scheme the carboxylate nucleophile and Mg^{2+}–pyrophosphate leaving group approach and depart from apical positions as the reaction proceeds through a pentacovalent transition state. As pointed out by Leatherbarrow et al. (1985), the first half of the reaction involves attack of a fully ionized nucleophile and departure of a good leaving group, suggesting that direct participation by enzyme functional groups may be unnecessary. By this scenario the role of the enzyme is to properly orient the ATP and amino acid substrates and to selectively bind the pentacovalent transition state, thus lowering the activation energy barrier of the reaction.

The crystal structure of GlnRS complexed with $tRNA^{Gln}$ and ATP clearly supports the in-line displacement mechanism for amino acid activation, as the proposed glutamine binding

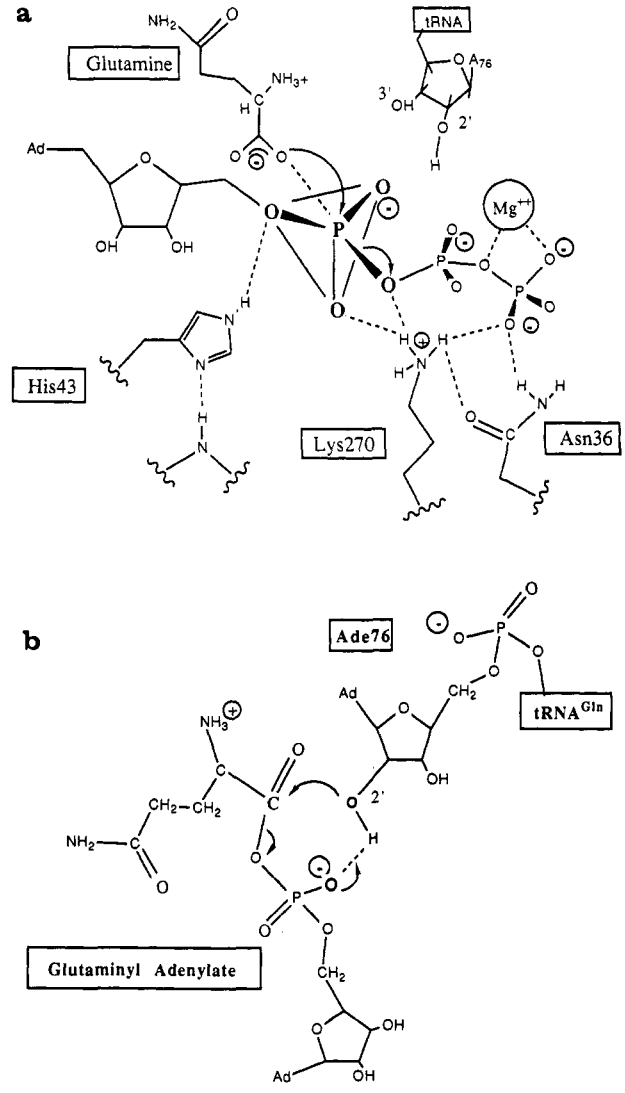

FIGURE 13: (a) Schematic view of a modeled transition state for the activation of glutamine to form glutaminyl adenylate, with concomitant formation of pyrophosphate. The model assumes that the network of interactions which stabilize the conformation of the β- and γ-phosphates of ATP (Figures 4–6) will render these groups relatively fixed during passage from the ground to the transition state at the α-phosphorus. Accordingly, the position of the bridging oxygen between the α- and β-phosphates was fixed, and one carboxylate oxygen of glutamine was positioned 180° opposite about the α-phosphorus atom, as required for the trigonal bipyramidal transition-state geometry. This model requires a conformational change of the ribose ring and possibly the adenine ring of ATP to relieve steric hindrance by the C5′ carbon (see text). The positions of the hydrogen atoms emanating from the terminal amine group of Lys270 were modeled by rotation about the Cϵ–Nζ bond to position one hydrogen midway between bridging and nonbridging oxygens of the α-phosphate (see text). The positions of the Asn36, His43, and Lys270 side chains (with the exception of the Lys270 hydrogens), the A_{76} nucleotide, Mg^{2+}, and the ATP phosphates are all directly determined from experimental electron density maps (e.g., Figures 1 and 7). Specific interactions proposed for Lys270, His43, and Asn36 in stabilizing the pentacovalent transition state are shown. No interaction of the α-phosphate of ATP with the A_{76} tRNA ribose group is shown owing to the unfavorable hydrogen-bonding geometry. (b) Mechanism of formation of glutaminyl-$tRNA^{Gln}$, with concomitant formation of the AMP product. Proposed intramolecular catalysis involving the action of the phosphate of the glutaminyl adenylate intermediate as a general base is shown.

site positions the α-carboxylate of this ligand on the opposing side of the α-phosphorus relative to the pyrophosphate leaving group (Figure 9). Inspection of the active site does not reveal specific enzyme moieties likely to function directly as acid–base or covalent catalysts, in agreement with conclusions

reached for the mechanism of TyrRS on the basis of the crystal structure (Brick & Blow, 1987) and of mutagenesis and kinetic analyses (Fersht, 1987). In fact, the position of the α-carboxylate of the glutamine in close proximity to the negatively-charged α-phosphate itself helps promote the structural transition of the α-phosphorus from a tetrahedral ground state to a trigonal bipyramidal transition-state geometry (Figure 9). This is due to the fact that, in order to form the planar arrangement about the α-phosphorus atom which is characteristic of the transition state (Figure 13a), the two nonesterified oxygens must move away from the attacking position of the negatively-charged carboxylate of glutamine. This movement is favored by the close proximity of the two negative charges.

Stabilization of the Transition State by Lys270 and His43. To assess the possible roles of individual amino acid residues in preferentially stabilizing the transition state for synthesis of glutaminyl adenylate, a model of this pentacovalent structure has been built on the basis of the observed positions of groups in the crystal structure of the ternary complex (Figure 13a). The major assumption made in the construction of this model is that the function of the network of interactions observed between enzyme groups and the β- and γ-phosphates of the ATP is to fix the position of the leaving pyrophosphate moiety (Figures 4–6). This contrasts with the proposal by Fersht and colleagues (Leatherbarrow et al., 1985) that the pyrophosphate moves significantly to interact with various residues in the transition state for synthesis of tyrosyl adenylate by TyrRS. We suggest instead that it is stereochemically more plausible that the enzyme fixes the position of the β- and γ-phosphates and that the small motion required to form the transition state may involve mainly the two nonbridging and the bridging 5′-oxygen joined to the α-phosphorus atom.

As noted above, when the substrate glutamine side chain is positioned in the available enzyme cavity, the attacking carboxylate group is mispositioned with respect to the α-phosphorus atom of the ATP. We therefore constructed the transition-state model by repositioning one glutamine carboxylate oxygen directly in-line with the bond connecting the α-phosphorus and the oxygen which bridges the α- and β-phosphates (Figure 13a). The positions of the two nonesterified oxygens and the bridging 5′-oxygen were then adjusted manually so as to achieve a pentacoordinate structure about the α-phosphorus, in which the O–P–O bond angles between apical and equatorial oxygens are 90° and O–P–O bond angles between two equatorial oxygens are 120° (Figure 13a). Fixing the pyrophosphate then imposes a requirement for at least a small rearrangement of the ribose ring to accommodate the altered directionality of the bond between the C5′- and O5′-atoms. A conformational change involving the ATP ribose group is also indicated by the fact that the position of the C5′-carbon atom is in close steric contact (1.9 Å) with the model-built nucleophilic oxygen of the glutamine α-carboxylate.

In the quaternary complex GlnRS-tRNA–ATP–glutamine, the interactions made by ATP are thus likely to differ somewhat from those seen in this ternary complex. We suggest that the differences are likely to reside in the contacts made by the ribose and adenine rings. Possibly, these groups might be displaced from their present positions to a location more similar to that seen for these moieties bound to TyrRS (Figure 11), in order to accommodate interactions made by the glutamine side chain. Significantly, the superposition of the GlnRS and TyrRS ligands shows that the C5′-carbon of tyrosyl adenylate is displaced away from the position of the glutamine carboxylate, as required to relieve the close steric contact. Also consistent is the observation that the region of polypeptide backbone of GlnRS contacting the adenine ring (residues 260–262, Figure 3) is at the beginning of a surface loop and does not make strong interactions with other enzyme groups. This section of backbone could thus possess the necessary flexibility to allow movement of the adenine and ribose rings of ATP; such flexibility exists in the TyrRS enzyme as seen in a comparison of structures of this enzyme complexed to tyrosine and to tyrosyl adenylate (see above). Additionally, the side chain of Arg260 which stacks upon the adenine ring is mobile and possesses multiple orientations, possibly allowing easier movement.

Inspection of the transition-state model permits a specific proposal for the roles of Lys270 and His43 of the conserved KMSKS and HIGH motifs in stabilizing the pentacovalent transition state of the α-phosphate during the synthesis of glutaminyl adenylate (Figure 13a). In the ternary complex of GlnRS-tRNA^{Gln}–ATP, the side-chain nitrogen of Lys270 is observed to lie within hydrogen-bonding distance of the α- and γ-phosphates of the ATP (Figures 4 and 6). It is thus positioned to directly stabilize the second negative charge on the α-phosphate which develops during the transition state (Figures 4, 6, 9, and 13a). Rotation about the Cε–Nζ bond of Lys270 allows the modeling of one hydrogen atom midway between the nonbridging and bridging oxygens of the α-phosphate (Figure 13a). While this O–P–O bond angle is initially the tetrahedral 109°, in the pentacovalent transition state it becomes 90° (Figure 13a). Positioning a hydrogen atom such that it makes this bifurcated interaction with two oxygens may stabilize an otherwise unfavorable decrease of the distance between them. The modeling also shows that the transition-state hydrogen bond distances between Nζ270 and these phosphate oxygens become shorter and the N—H···O angles become more linear; thus, the interactions stabilize the pentacovalent transition-state relative to the ground-state tetrahedral phosphate. It was not possible to postulate such a direct role for this conserved lysine from the TyrRS structure due to the disorder of the mobile loop in which it rests as well as the fact that the complex with ATP was not studied.

The protonated nitrogen of the imidazole ring of His43 also lies adjacent to the α-phosphate on the side opposite the terminal tRNA ribose (Figures 4 and 13a). This nitrogen is positioned approximately 3.5 Å distant from both bridging and one nonbridging oxygen of the α-phosphate, suggesting that the residue contributes little binding energy in the ground state. However, movement of the O5′ oxygen linking the α-phosphate and ribose ring toward the equatorial position of the pentacovalent transition state is in the direction of the imidazole ring, leading us to propose that this side chain also contributes selectively to transition-state stabilization (Figures 4, 6, 9, and 13a).

This proposed role of Lys270 in stabilizing the transient pentacovalent species is analogous to the effect of an ethylene bridge on methyl ester hydrolysis of methyl ethylene phosphate. The rate of hydrolysis of methyl ethylene phosphate is accelerated by a factor of 10^6 relative to that of the trimethyl analog (Westheimer, 1968), presumably because the ethylene bridge strains the O–P–O bond angle to 99°, 10° less than the tetrahedral angle (Steitz & Lipscomb, 1965). Thus, the ethylene group reduces the energy required to form a 90° O–P–O bond angle between the apical and equatorial oxygens in the transition state. Similarly, the interaction of a hydrogen atom of Nζ270 with analogous oxygens of the α-phosphate of ATP reduces the energy required to draw these oxygens

closer together in the transition state.

The function hypothesized for the positively-charged ϵ-amino group of Lys270 may also be analogous to the role postulated for one divalent metal ion in several phosphoryl transfer reactions. In the case of the 3′–5′ exonuclease active site of *E. coli* DNA polymerase I (Freemont et al., 1988; Beese & Steitz, 1991) and in *E. coli* alkaline phosphatase (Kim & Wyckoff, 1991), a divalent metal ion bridges the leaving group phosphate oxygen (which is apical in the transition state) and a nonbridging phosphate oxygen (which becomes equatorial in the transition state). Apparently either a divalent metal ion or a lysine ϵ-amino group can be used for this stabilizing function. There are also examples in which arginine residues have been shown to stabilize a nearly identical pentacovalent transition state (e.g., the phosphomonoesterases *E. coli* alkaline phosphatase (Kim & Wyckoff, 1991) and rat liver fructose-2,6-bisphosphatase (Lin et al., 1992)), although the precise manner in which a guanidinium group preferentially interacts with the bridging and nonbridging oxygens is likely to differ.

Asn36 appears to play a subsidiary role in stabilizing the orientation of the side chain of Lys270 for its function in transition-state stabilization (Figures 5, 6, and 13a). In the ternary complex crystal structure, we observe a hydrogen bond between the amine nitrogen of Lys270 and the side-chain amide oxygen of Asn36 (Figure 5). Positioning one hydrogen of the Lys270 NH_3^+ group directly in-line to Asn36 results in a second hydrogen being located directly between bridging and nonbridging oxygens of the α-phosphate in the transition-state model (Figure 13a). This suggests that Asn36 may stabilize the transition state indirectly by virtue of its ability to stabilize a rotamer of Lys270 in which a single hydrogen makes a bifurcated interaction with the α-phosphate. The amino group of the Asn36 side chain also interacts directly with the γ-phosphate (Figure 5). A further interaction in this region is made by the main-chain amide of Glu34 with the α-phosphate of ATP (Figure 6). However, a comparison of the pentacovalent transition-state model with the crystal structure shows that the strength of this hydrogen bond, as assessed by distance and deviation from linearity, is likely to be weaker in the transition state.

The Mg^{2+} ion bridging the β- and γ-phosphates plays a complementary role in assisting the reaction by withdrawing electrons and (together with enzyme groups) in facilitating adoption of a productive conformation of the pyrophosphate. The proposed Mg^{2+} binding site is identical to that described for other synthetases, including TyrRS (Connolly et al., 1980; Smith & Cohn, 1982; Piel et al., 1983; Garcia et al., 1990).

Based on the crystal structure and the modeling of the transition state, we therefore predict that Lys270, His43, and Asn36 of GlnRS function to preferentially stabilize the transition state relative to the ground state. These inferences are in accord with mutagenesis and kinetic data on TyrRS, which show that the homologous residues Lys233, His48, and Thr40 all stabilize the transition state for synthesis of tyrosyl adenylate (Wells & Fersht, 1985; Leatherbarrow et al., 1985; Fersht et al., 1988). His45 of TyrRS was similarly proposed to stabilize the transition state in that enzyme. The equivalent His40 of GlnRS interacts with the β-phosphate of ATP indirctly through a water molecule; it is unclear whether it might preferentially stabilize the ground or transition state in GlnRS. Further comparisons of the roles of the structurally equivalent amino acids in the active sites of the two enzymes require kinetic data on the behavior of analogous GlnRS mutants and/or structural data delineating the interactions of the β- and γ-phosphates of ATP with TyrRS. Additionally, it is clear that hypotheses regarding the functions of the various active site residues derived from kinetic data would be strengthened considerably by structural information on the mutant enzymes.

Participation of $tRNA^{Gln}$ in Synthesis of Glutaminyl Adenylate. GlnRS requires bound tRNA in order to synthesize glutaminyl adenylate, an unusual requirement shared by only two other synthetases, GluRS and ArgRS (Schimmel & Söll, 1979). The 2′-oxygen of the terminal tRNA adenosine lies 2.7 Å from a nonbridging oxygen of the α-phosphate (Figures 5, 6, and 9). However, the hydrogen atom bonded to this ribose oxygen is located such that the O—H···O hydrogen-bonding angle is approximately 90°, making it unlikely that the interaction has significant hydrogen-bonding character. This angle improves only slightly in the transition-state model. It is thus difficult to explain the observation that use of $tRNA^{Gln}$ containing a 2′-deoxy modification at the ribose of A_{76} completely abolishes GlnRS activity in an ATP–PP_i exchange reaction monitoring incorporation of labeled pyrophosphate into ATP (Englisch-Peters et al., 1991). Removal of a single stabilizing interaction would in any event be expected to reduce but not fully abolish the ability of the enzyme to carry out this reaction. Possibly, the A_{76} 2′-OH group plays a pivotal role in bringing about a local conformational change necessary to the productive simultaneous binding of ATP and glutamine. As described above, it appears that at least a small rearrangement of the ATP ribose group from its observed position is a feature of the quaternary E-tRNA–ATP–glutamine ground-state complex.

Second Step of the Aminoacylation Reaction. In the second step of the aminoacylation of $tRNA^{Gln}$, a nucleophilic hydroxyl group of the terminal tRNA ribose attacks the carbonyl carbon of the mixed anhydride intermediate, forming a tetrahedral transition state, thereby generating an incipient negative charge on the carbonyl oxygen atom (Figure 13b). Although there is no obvious compensatory positive charge nearby in the present structure, an alternative mechanism for aiding the reaction could be by directly increasing the nucleophilicity of the 2′-ribose hydroxyl group. The observation that the 2′-OH group of the ribose and the α-phosphate of ATP lie adjacent to each other suggests a possible mechanism for assisting formation of glutaminyl-$tRNA^{Gln}$: one of the negatively-charged α-phosphate oxygens of the glutaminyl adenylate intermediate itself could function as a general base in the reaction by abstracting the proton from the 2′-OH ribose group. While intramolecular catalysis in enzymes is uncommon, a similar mechanism has been proposed for the enzyme aspartate carbamoyltransferase (Gouaux et al., 1987; Gouaux & Lipscomb, 1988). In this case, it is proposed that the intermediate carbamoyl phosphate catalyzes its own decomposition, with a phosphate oxygen abstracting a proton from the amino group of aspartate.

As described above, the juxtaposition of the negative charges of the glutamine carboxylate and the α-phosphate of ATP itself helps promote movement toward the first transition state of the aminoacylation reaction. Therefore, the two halves of the reaction resemble each other in an important respect—in each step the structures of the substrates and intermediates themselves are such as to favor the forward progress of the reaction. In fact, it appears that the function of almost all of the amino acids at the synthetase active site is to correctly orient the substrates; some of these—such as Lys270 and His43—will further preferentially interact with one or both of the transition states. This suggests that in a primordial cell

the coupling of amino acids to an adaptor molecule composed of nucleic acid could be in principle feasible without the intervention of highly evolved enzymic catalysts. Possibly, an RNA-based synthetase could have achieved all of the functions now exhibited by this enzyme. In this scenario the roles of Lys270 and His43 could well have been played by a properly oriented magnesium ion.

Lastly, it is of interest to consider the fact that most synthetases discriminate among the structurally similar tRNAs in the cell primarily on the basis of k_{cat} rather than K_M (Schimmel & Söll, 1979). The structure of GlnRS complexed to $tRNA^{Gln}$ suggests at least two distinct mechanisms by which this may be acheived: (i) anticodon loop recognition coupled to a conformational transition of the KMSKS loop and (ii) recognition in the minor groove of the acceptor stem coupled to binding of the ATP ribose group (Figure 2). Interestingly, it is precisely those nucleotides of the tRNA implicated as identity elements (Perona et al., 1989; Rould et al., 1991; Jahn et al., 1991) which may also be involved in promoting structural changes required for efficient catalysis. Coupling of tRNA selectivity directly to the construction of a catalytically proficient active site represents an elegant solution to the problem of discrimination among some 80 separate tRNA species, all of which possess the common L-shaped tertiary structure. Similar mechanisms are doubtless present in many of the aminoacyl-tRNA synthetases.

REFERENCES

Bedouelle, H., & Winter, G. (1986) *Nature 320*, 371–373.

Beese, L. S., & Steitz, T. A. (1991) *EMBO J. 10*, 25–33.

Breton, R., Sanfacon, H., Papayannapoulos, I., Biemann, K., & LaPointe, J. (1986) *J. Biol. Chem. 261*, 10610–10617.

Brick, P., & Blow, D. M. (1987) *J. Mol. Biol. 194*, 287–297.

Brick, P., Bhat, T. N., & Blow, D. M. (1989) *J. Mol. Biol. 208*, 83–98.

Brunger, A. T. (1988) *J. Mol. Biol. 203*, 803.

Brunie, S., Zelwer, C., & Risler, J.-L. (1990) *J. Mol. Biol. 216*, 411–424.

Carter, P., Bedouelle, H., & Winter, G. (1986) *Proc. Natl. Acad. Sci. U.S.A. 83*, 1189–1192.

Connolly, B. A., Von der Haar, F., & Eckstein, F. (1980) *J. Biol. Chem. 255*, 11301–11307.

Cullis, P. M. (1987) Acyl Group Transfer—Phosphoryl Transfer, in *Enzyme Mechanisms* (Page, M. I., & Williams, A. Eds.) pp 178–220, Royal Society of Chemistry, London.

Cusack, S., Berthet-Colominas, C., Hartlein, M., Nassar, N., & Leberman, R. (1990) *Nature 347*, 249–255.

Englisch-Peters, S., Conley, J., Plumbridge, J., Leptak, C., Söll, D., & Rogers, M. J. (1991) *Biochimie 73*, 1501–1508.

Eriani, G., Dirheimer, G., & Gangloff, J. (1989) *Nucleic Acids Res. 17*, 5725–5736.

Eriani, G., Delarue, M., Poch, O., Gangloff, J., & Moras, D. (1990) *Nature 347*, 203–206.

Eriani, G., Dirheimer, G., & Gangloff, J. (1991) *Nucleic Acids Res. 19*, 265–269.

Fersht, A. R. (1987) *Biochemistry 26*, 8031–8037.

Fersht, A. R., Knill-Jones, J. W., Bedouelle, H., & Winter, G. (1988) *Biochemistry 27*, 1581.

Freemont, P. S., Friedman, J. M., Beese, L. S., Sanderson, M. R., & Steitz, T. A. (1988) *Proc. Natl. Acad. Sci. U.S.A. 85*, 8924–8928.

Garcia, G. A., Leatherbarrow, R. J., Eckstein, F., & Fersht, A. R. (1990) *Biochemistry 29*, 1643–1648.

Gouaux, J. E., & Lipscomb, W. N. (1988) *Proc. Natl. Acad. Sci. U.S.A. 85*, 4205–4208.

Gouaux, J. E., Krause, K. L., & Lipscomb, W. N. (1987) *Biochem. Biophys. Res. Commun. 142*, 893–897.

Haertlein, M., Frank, R., & Madern, D. (1987) *Nucleic Acids Res. 15*, 9081–9082.

Hall, C. V., van Cleemput, M., Muench, K. H., & Yanofsky, C. (1982) *J. Biol. Chem. 257*, 6132–6136.

Jahn, M., Rogers, M. J., & Söll, D. (1991) *Nature 352*, 258–260.

Kim, E. E., & Wyckoff, H. W. (1991) *J. Mol. Biol. 218*, 449–464.

Labouze, E., & Bedouelle, H. (1989) *J. Mol. Biol. 205*, 729–735.

Landes, C., Perona, J. J., Brunie, S., Rould, M. A., Steitz, T. A., Zelwer, C., & Risler, J.-L. (1993) *J. Mol. Biol.* (submitted for publication).

Leatherbarrow, R. J., & Fersht, A. R. (1986) *Protein Eng. 1*, 7.

Leatherbarrow, R. J., Fersht, A. R., & Winter, G. (1985) *Proc. Natl. Acad. Sci. U.S.A. 82*, 7840–7844.

Lin, K., Li, L., Correia, J. J., & Pilkis, S. J. (1992) *J. Biol. Chem. 267*, 19163–19171.

Lowe, G., & Tansley, G. (1984) *Tetrahedron 40*, 113–117.

Mechulam, Y., Dardel, F., LeCorre, D., Blanquet, S., & Fayat, G. (1991) *J. Mol. Biol. 217*, 465–475.

Perona, J. J., Swanson, R., Rould, M. A., Steitz, T. A., & Söll, D. (1989) *Science 246*, 1152–1154.

Perona, J. J., Rould, M. A., Steitz, T. A., Risler, J.-L., Zelwer, C., & Brunie, S. (1991) *Proc. Natl. Acad. Sci. U.S.A. 88*, 2903–2907.

Piel, N., Freist, W., & Cramer, F. (1983) *Bioorg. Chem. 12*, 18–33.

Rossmann, M. G., & Argos, P. (1976) *J. Mol. Biol. 105*, 75–95.

Rould, M. A., Perona, J. J., Söll, D., & Steitz, T. A. (1989) *Science 246*, 1135–1142.

Rould, M. A., Perona, J. J., & Steitz, T. A. (1991) *Nature 352*, 213–218.

Ruff, M., Krishnaswamy, S., Boeglin, M., Poterszman, A., Mitschler, A., Podjarny, A., Rees, B., Thierry, J. C., & Moras, D. (1991) *Science 252*, 1682–1689.

Schimmel, P. (1987) *Annu. Rev. Biochem. 56*, 125.

Schimmel, P. R., & Söll, D. (1979) *Annu. Rev. Biochem. 48*, 601–648.

Smith, L. T., & Cohn, M. (1982) *Biochemistry 21*, 1530–1534.

Steitz, T. A., & Lipscomb, W. N. (1965) *J. Am. Chem. Soc. 87*, 2488–2489.

Webster, T., Tsai, H., Kula, M., Mackie, G. A., & Schimmel, P. (1984) *Science 226*, 1315.

Wells, T. N. C., & Fersht, A. R. (1985) *Nature 316*, 656–657.

Westheimer, F. H. (1968) *Acc. Chem. Res. 1*, 70–78.